VII International Conference on Particle-Based Methods
PARTICLES 2021
P. Wriggers, M. Bischoff, E. Oñate, M. Bischoff, A. Düster & T. Zohdi (Eds)

UPSCALING BETWEEN AN AGENT-BASED MODEL (SMOOTHED PARTICLE APPROACH) AND A CONTINUUM-BASED MODEL FOR SKIN CONTRACTIONS IN ONE DIMENSION

Q. Peng[1,2], **F. J. Vermolen**[2,1]

[1] Delft Institute of Applied Mathematics
Delft University of Technology
Mekelweg 4, 2628 CD, Delft, The Netherlands
e-mail: Q. Peng-1@tudelft.nl

[2] Computational Mathematics Group, Discipline Group Mathematics and statistics
Faculty of Science, Hasselt University
Campus Diepenbeek, Agoralaan Gebouw D, BE 3590, Diepenbeek, Belgium
email: Fred.Vermolen@uhasselt.be

Key words: Force balance, Mechanics, Smoothed Particle Approach, Agent-Based Modelling, Finite Element Methods, Continuum-Based Modelling

Abstract. Skin contraction during wound healing is mainly caused by fibroblasts (skin cells) and myofibroblasts (differentiated fibroblasts) that exert pulling forces on the surrounding extracellular matrix (ECM). Modelling is done in multiple scales: agent–based modelling on the microscale and continuum–based modelling on the macroscale. The momentum equilibrium equation is used to simulate this phenomenon in both models, with different expression of the cellular forces. In this manuscript, we managed to rigorously establish the link between the two modelling approaches for both closed–form solutions and finite–element approximations in one dimension.

1 Introduction

Wound healing is a spontaneous process for the skin to cure itself after an injury. In the proliferation phase, the scar will contract since the regular fibroblasts start proliferating and exert forces on the extracellular matrix (ECM). For superficial wounds that only concern epidermis, the wound can be healed without any problem. However, for severe injuries, in particular, in dermal wounds, scar may contract so much that it will cause disabilities and disfunctioning of joints. If this happens, then one speaks of a contracture. Contractures are recognized as excessive and problematic contractions, which occur due to the pulling forces exerted by the (myo)fibroblasts on ECM. Usually, $5-10\%$ reduction of wound area has been observed in clinical trials. A more detailed biological description can be found in Cumming et al. [1], Enoch and Leaper [2], Haertel et al. [3], Martin [4].

In our previous work [5], a formalism to describe the mechanism of the displacement of the ECM in agent-based model has been used, which is firstly developed by Boon et al. [6] and improved further by Koppenol [7]. Regarding the elasticity equation with point forces, we realized that the solution to the partial differential equation is singular for dimensionality exceeding one. Hence, we developed various alternatives to improve the accuracy of the solution in [8, 9].

We have been working with agent-based models so far, which model the cells as individuals and define the formalism of pulling forces by superposition theory. However, once the wound scale is larger, the agent-based model is increasingly expensive from a computational perspective, and hence, the cell density model is preferred, which considers many cells as one collection in a unit. In this manuscript, we investigate and discover the connections between these two models in one dimension as the exact solutions are available, in the perspective of modelling the mechanism of pulling forces exerted by the (myo)fibroblasts. As the consistency between the smoothed particle approach (SP approach) and the immersed boundary approach has been proven both analytically and numerically [8, 9], we select the SP approach here due to its continuity and smoothness, to compare with the cell density model using finite-element methods.

The manuscript is structured as follows. We start introducing both models in Section 2. Section 3 displays both the exact solutions and the numerical results using finite-element methods. Finally, some conclusions are shown in Section 4.

2 Mathematical Models

Considering one-dimensional force equilibrium, the equations are given by

$$\begin{aligned} -\frac{d\sigma}{dx} &= f, && \text{Equation of Equlibirum,} \\ \epsilon &= \tfrac{du}{dx}, && \text{Strain-Displacement Relation,} \\ \sigma &= E\epsilon, && \text{Constitutive Equation.} \end{aligned}$$

By substituting $E = 1$, the equations above can be combined to Laplacian equation in one dimension:

$$-\frac{d^2u}{dx^2} = f. \tag{1}$$

2.1 Smoothed Particle Approach

In Peng and Vermolen [9], a smoothed particle approach (SP approach) is developed as an alternative of the Dirac Delta distribution describing the point forces exerted by the biological cells, in the application of wound healing:

$$(BVP_{SP}) \begin{cases} -\dfrac{d^2u}{dx^2} = P_{SP} \displaystyle\sum_{i=1}^{N_s} \delta'_\varepsilon(x - s_i), x \in (0, L), \\ u(0) = u(L) = 0, \end{cases} \tag{2}$$

where P_{SP} is the magnitude of the forces, $\delta_\varepsilon(x)$ is the Gaussian distribution with variance ε and s_i is the centre position of biological cell i. One can solve the partial differential equations (PDEs) with finite-element methods. The corresponding weak form is given by

$$(WF_{\mathrm{SP}}) \begin{cases} \text{Find } u \in H_0^1((0,L)), \text{ such that} \\ \displaystyle\int_0^L u'\phi' dx = \int_0^L \sum_{i=1}^{N_s} P_{SP}\delta'_\varepsilon(x-s_i)\phi dx, \text{ for all } \phi \in H_0^1((0,L)). \end{cases}$$

Without this knowledge, the existence and uniqueness of the H_0^1-solution follows as well from the application of the Lax–Milgram theorem [10], where it is immediately obvious that the bilinear form in the left–hand side is symmetric and positive definite.

2.2 Cell Density Approach

A cell density approach is often used in the large scale, so that the computational efficiency is much improved compared with the agent-based model. According to the model in Koppenol [7], the force in two dimensions can be determined by the divergence of $n_c \cdot \boldsymbol{I}$, where n_c is the local density of the biological cells and $\boldsymbol{I}$ is the identity tensor. In one dimension, the cell density approach is expressed as:

$$(BVP_{den}) \begin{cases} -\dfrac{d^2u}{dx^2} = P_{den}\dfrac{dn_c}{dx}, x \in (0,L), \\ u(0) = u(L) = 0, \end{cases} \tag{3}$$

where P_{den} is the magnitude of the forces. The corresponding weak form is given by

$$(WF_{\mathrm{den}}) \begin{cases} \text{Find } u \in H_0^1((0,L)), \text{ such that} \\ \displaystyle\int_0^L u'\phi' dx = \int_0^L P_{den} n'_s \phi dx, \text{ for all } \phi \in H_0^1((0,L)). \end{cases}$$

2.3 Consistency between Two Models

2.3.1 Analytical Solutions with Specific Locations of Biological Cells

To express the analytical solution, it is necessary to determine the locations of the biological cells, such that the cell density can be written as an analytical function of the positions. We assume, there are N_s cells distributed uniformly in the subdomain (a,b) of the computational domain $(0,L)$. Hence, the distance between the center position of any two adjacent biological cells is constant, which we denote $\Delta s = (b-a)/N_s$ and the first and the N_s-th cell are located at $x = a + \Delta s/2$ and $x = b - \Delta s/2$, respectively. With homogeneous Dirichlet boundary conditions, and suppose $P_{SP} = P\Delta s$ and variance $\varepsilon = \Delta s$, the boundary value problem of the SP approach is expressed as

$$(BVP^1_{SP}) \begin{cases} -\dfrac{d^2u_1}{dx^2} = P\Delta s \displaystyle\sum_{i=1}^{N_s} \delta'_{\Delta s}(x-s_i), x \in (0,L), \\ u_1(0) = u_1(L) = 0, \end{cases} \tag{4}$$

where P is a positive constant and s_i is the centre position of the biological cells. Utilizing the superposition principle, the analytical solution is given by

$$u_1(x) = P\Delta s \sum_{i=1}^{N_s} \frac{1}{2}\left\{\left(\frac{x}{L}-1\right)\text{erf}\left(\frac{s_i}{\sqrt{2}\Delta s}\right) + \frac{x}{L}\,\text{erf}\left(\frac{L-s_i}{\sqrt{2}\Delta s}\right) - \text{erf}\left(\frac{x-s_i}{\sqrt{2}\Delta s}\right)\right\}, \quad (5)$$

where $\text{erf}(x)$ is the error function defined as $\text{erf}(x) = \frac{2}{\sqrt{\pi}}\int_0^x \exp(-t^2)dt$ [11]. Since the biological cells are uniformly located between a and b ($0 < a < b < L$), $\frac{dn_c}{dx}$ can be rephrased as

$$\frac{dn_c}{dx} = \begin{cases} \frac{1}{t}, & a - \frac{t}{2} < x < a + \frac{t}{2}, \\ -\frac{1}{t}, & b - \frac{t}{2} < x < b + \frac{t}{2}, \\ 0, & \text{otherwise}, \end{cases}$$

where t is a small positive constant. Taking t to zero, the above expression converges to $\delta(x-a) - \delta(x-b)$. Hence, the boundary value problem of the cell density model can be written as

$$(BVP^1_{den}) \begin{cases} -\frac{d^2u_2}{dx^2} = P\frac{dn_c}{dx} \to P(\delta(x-a) - \delta(x-b)), x \in (0, L), \\ u_2(0) = u_2(L) = 0, \end{cases} \quad (6)$$

where $\delta(x)$ is the Dirac Delta distribution and a and b are the left and right endpoint of the subdomain (where biological cells are uniformly located) respectively. The analytical solution is then expressed as

$$u_2(x) = P(G(x,a) - G(x,b)), \quad (7)$$

where $G(x, x')$ is the Green's function [12], defined by

$$G(x,x') = (1 - \frac{x'}{L})x - max(x - x', 0),$$

in the computational domain $(0, L)$.

Actually, the convergence between $u_1(x)$ and $u_2(x)$ can be proven as $\Delta s \to 0^+$ by a proposition; see more details regarding the proof in Peng and Vermolen [13].

Proposition 1. *Let $u_1(x)$ as described in Eq (4) be the exact solution to (BVP^1_{SP}) and $u_2(x)$ as described in Eq (6) be the exact solution to (BVP^1_{den}). As $\Delta s \to 0^+$, $u_1(x)$ converges to $u_2(x)$.*

2.3.2 Finite-Element Method Solutions with Arbitrary Locations of Biological Cells

For the finite-element method, we select the piecewise Lagrangian linear basis functions. We divide the computational domain into N_e mesh elements, with the nodal point $x_1 = 0$

and $x_{N_e+1} = L$. For the implementation, we define the cell density as the count of biological cell in every mesh element divided by the length of the mesh element, hence, it is a constant within every mesh element. In other words, in the mesh element $[x_j, x_{j+1}]$, the count of the biological cell is defined by

$$N_c([x_j, x_{j+1}]) = \int_{x_j}^{x_{j+1}} n_c([x_j, x_{j+1}])dx = hn_c([x_j, x_{j+1}]),$$

for any $j \in \{1, \ldots, N_e\}$, where h is the size of every mesh element. Different from (BVP^1_{SP}) where Δs is the variance of δ_ε, for finite-element methods, we set $\varepsilon = h/3$, such that the integration of $\delta_{h/3}(x - x')$ for any $0 < x' < L$ over any mesh element with size h, is close to 1 (see Peng and Vermolen [13]). With the two approaches, the boundary value problems with Dirichlet boundary condition are defined by

$$(BVP^2_{SP}) \begin{cases} -\dfrac{d^2u_1}{dx^2} = Ph\displaystyle\sum_{i=1}^{N_s} \delta'_{h/3}(x - s_i), x \in (0, L), \\ u_1(0) = u_1(L) = 0, \end{cases} \tag{8}$$

and

$$(BVP^2_{den}) \begin{cases} -\dfrac{d^2u_2}{dx^2} = Ph\dfrac{dn_c}{dx}, x \in (0, L), \\ u_2(0) = u_2(L) = 0, \end{cases} \tag{9}$$

where s_i is the position of biological cells, h is the mesh size and N_s is the total number of cells in the computational domain. The consistency between (BVP^2_{SP}) and (BVP^2_{den}) can be verified by the following theorem, and the proof can be found in Peng and Vermolen [13].

Theorem 1. *Denote $u^h_1(x)$ and $u^h_2(x)$ respectively the solution to (BVP^2_{SP}) and (BVP^2_{den}). With Lagrangian linear basis functions for the finite element method, $u^h_1(x)$ converges to $u^h_2(x)$, as the size of the mesh element $h \to 0^+$, regardless of the positions of biological cells.*

3 Results

Since the objective of this manuscript is to investigate the consistency and the connections between the SP approach and the cell density approach, all the parameters are dimensionless.

We show the results by analytical solutions in Figure 1 with various values of Δs (i.e. depending on different number of biological cells in the subdomain (a, b)). Here, the computational domain is $(0, 7)$ with $L = 7$ and the subdomain where the biological cells locate uniformly is $(2, 5)$ with $a = 2$ and $b = 5$. With the decrease of the variance in the Gaussian distribution in (BVP^2_{SP}), the curves gradually overlap, which verifies the convergence between the analytical solutions to these two approaches.

To implement the model, there are two different algorithms shown in Figure 2 and 3. Depending on different circumstances, the implementation method is elected. The cell

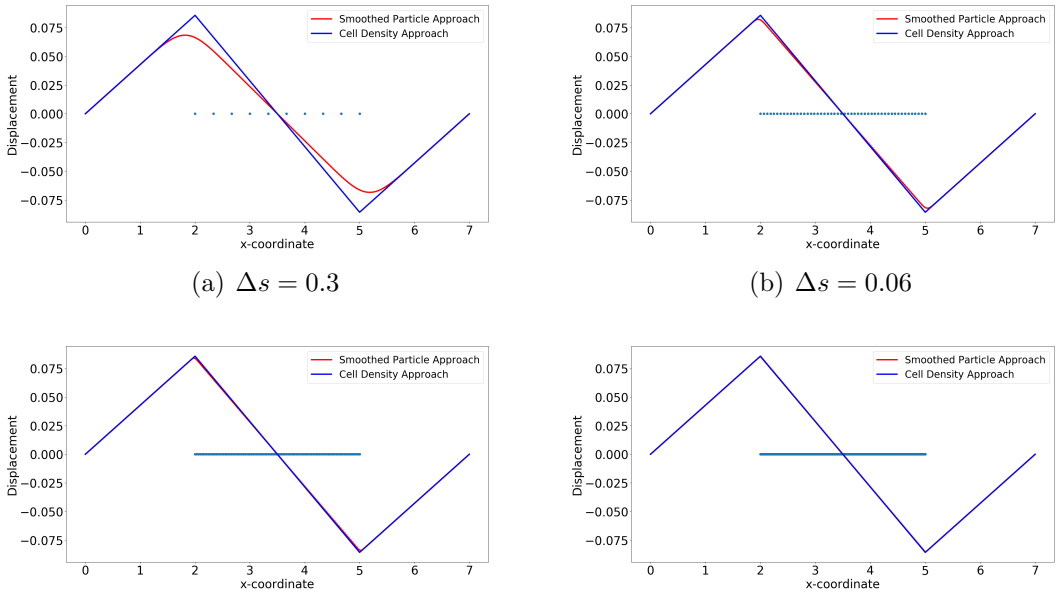

(a) $\Delta s = 0.3$ (b) $\Delta s = 0.06$

(c) $\Delta s = 0.03$ (d) $\Delta s = 0.006$

Figure 1: The exact solutions to (BVP^1_{SP}) and (BVP^1_{den}) are shown, with various values of Δs, which is the distance between centre positions of any two adjacent biological cells. Blue points are the centre positions of biological cells. Red curves represent the solutions to (BVP^1_{SP}) and blue curves represent the solutions to (BVP^1_{den}).

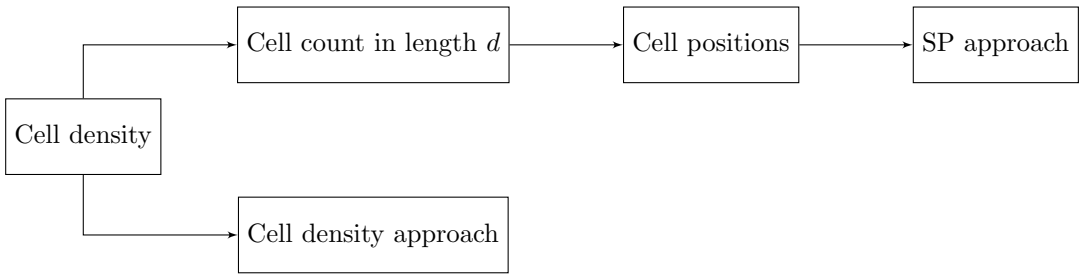

Figure 2: With exact expression of cell density function and the first order derivative of the function exists, cell density approach is implemented directly. Based on the cell density, the number of cells in a certain region with length d is determined and subsequently, the center positions of cells can be generalized. Hence, the SP approach is implemented.

density in one dimension is defined as the number of cells per length unit. In other words, the cell count in a given domain can be computed by integrating the cell density over the domain. If the cell density function can be expressed analytically and the first order derivative of the function exists, then a certain bin length d is chosen and the cell count in every bin of d length is calculated. Then we generalize the center positions of cells in every bin of length d, thus, the SP approach can be implemented, as it is indicated in Figure 2. However, it is not always straightforward to obtain the analytical expression of cell density. If the center positions of cells are given, the number of cells in each mesh

element can be counted, hence, the cell density will be computed analogously at each mesh points. Therefore, the boundary value problem of cell density approach is solved by numerical methods, for example, the finite-element methods.

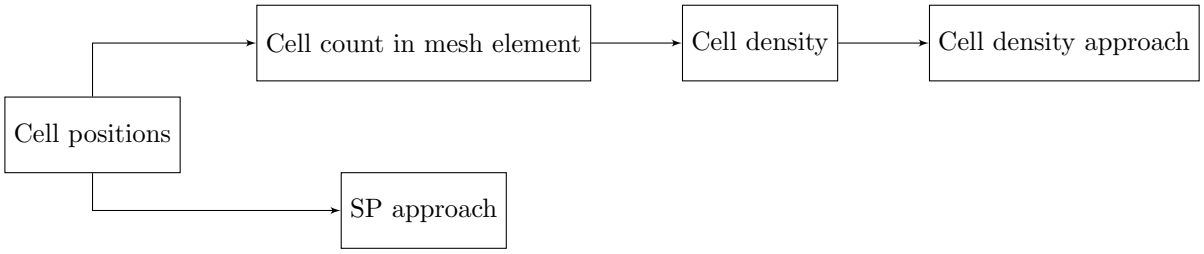

Figure 3: Given the center positions of cells, one can directly implement the SP model. Computing the number of cells in every mesh element and divided by the length of the mesh element results into the cell density. Subsequently, cell density approach can be implemented.

In this manuscript, all the numerical results are derived by finite-element methods with Lagrangian linear basis functions. Regarding the first implementation method (see Figure 2), we show the results with a Gaussian distribution and sine function as cell density functions; see Figure 4 and 5. We start with the simulations in which we keep the number of cells and the center positions of the cells the same, then we refine the mesh. In Figure 5(a)-(c), the bin length d is 0.35, and the mesh size is a function of d. The results solved by SP approach become smoother. With various values of d, the solutions to the approaches are overlapping only when the factor between the d and mesh size is closer to 1. From Figure 5(d) to (f), the mesh is fixed and we vary the value of d. We note that in Figure 5(f), the solution to the SP approach is significantly different from the solution to the cell density approach. It is mainly caused by the fact that d is too small and there is barely any fluctuation with the count of cells in every d length subdomain, while with the Gaussian distribution as the cell density function, the majority of the cells are centered around $x = 3.5$. Hence, the solution to SP approach still manages to be comparable with the solution to the cell density approach; see Figure 4(f). Numerical results of the simulation in Figure 4 are displayed in Table 1. There are some noticeable differences between two approaches, in particular the convergence rate in the H^1-norm: thanks to the given, differentiable cell density function, the cell density approach converges faster. In addition, the cell density approach requires less computational time with a factor of 15.

We consider cells that are located uniformly in the subdomain $(2, 5)$, which implies that the gradient or divergence of the cell density vanishes inside the subdomain but does not exist at two endpoints of the subdomain. Hence, we utilize the implementation method in Figure 3, as the center positions of the cells are given, then the local cell density can be calculated per unit area. Compared with the results shown in Figure 1, the results in Figure 6 and Figure 7 show the solutions to (BVP^2_{SP}) and (BVP^2_{den}) respectively. Note that, in the finite-element method solutions, the magnitude of the forces in both approaches are the same, and the variance of $\delta_\varepsilon(x)$ is related to h rather than Δs. Furthermore, these figures verify that the convergence between SP approach

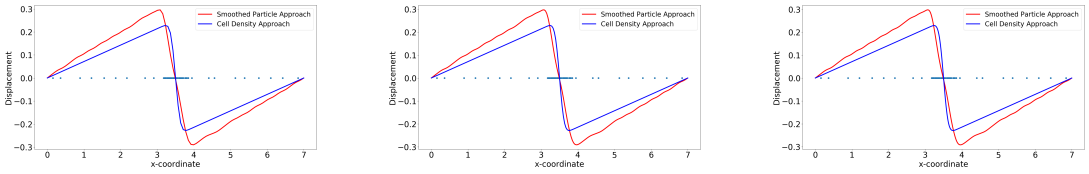

(a) $h(d) = d/5, h = 0.07, d = 0.35$ (b) $h(d) = d/10, h = 0.035, d = 0.35$ (c) $h(d) = d/50, h = 0.007, d = 0.35$

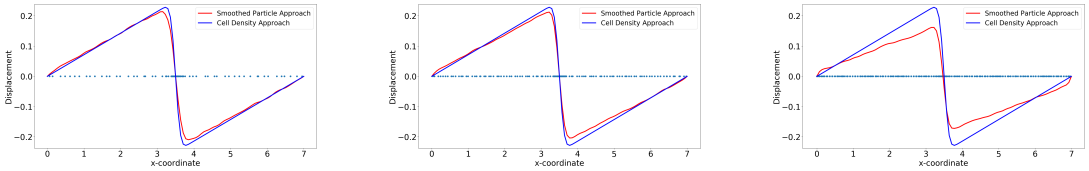

(d) $d(h) = 2h, h = 0.07, d = 0.14$ (e) $d(h) = h, h = 0.07, d = 0.07$ (f) $d(h) = h/4, h = 0.07, d = 0.0175$

Figure 4: The cell density function is Gaussian distribution and using the algorithm in Figure 2, different simulations are carried out with various mesh size and the total number of cells. Blue curves represent the solutions to (BVP^2_{SP}), and ref curves are the solutions to (BVP^2_{den}) with $n_c(x) = 50 \times 1/\sqrt{2\pi \times 0.1^2}\exp\{-(x-3.5)^2/(2\times 0.1^2)\}$. In Subfigure (a)–(c), we set $d = 0.35$ and cell positions are fixed, as h is decreasing. From Subfigure (d) to Subfigure (f), we use the same finite-element method settings (where h is sufficiently small with $h = 0.07$), and simulations are carried out with various values of d.

Table 1: Numerical results of two approaches in one dimension, where the cell density function is Gaussian distribution: $n_c(x) = 50 \times 1/\sqrt{2\pi \times 0.1^2}\exp\{-(x-3.5)^2/(2\times 0.1^2)\}$. Here, we define $N_s = 88$ and the mesh size $h = 0.07$. The results are solved by finite-element method with algorithm in Figure 2.

	SP Approach	**Cell Density Approach**
$\|u\|_{L^2((0,L))}$	0.544148107	0.361979308
$\|u\|_{H^1(((0,L))}$	0.964215173	0.871720645
Convergence rate of $L^2 - norm$	1.75281178	1.826378221
Convergence rate of $H^1 - norm$	1.70114233	1.716659924
Reduction ratio of the subdomain (a, b) (%)	13.88062	9.52381
Time cost (s)	0.045070	0.0032084

and cell density approach is determined by the mesh size rather than by the distance between any two adjacent cells. Table 2 displays the numerical results of the simulation in Figure 6, in the perspective of the solution, the reduction ratio of the subdomain and the computational cost. Similarly to the figures, there is no significant difference between the norms and the deformed length of the subdomain. However, the simulation time in the cell density approach is much shorter than in the SP approach with a factor of 35.

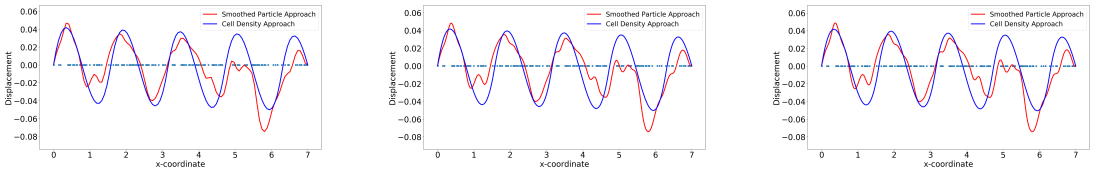

(a) $h(d) = d/5, h = 0.07, d = 0.35$ (b) $h(d) = d/10, h = 0.035, d = 0.35$ (c) $h(d) = d/50, h = 0.007, d = 0.35$

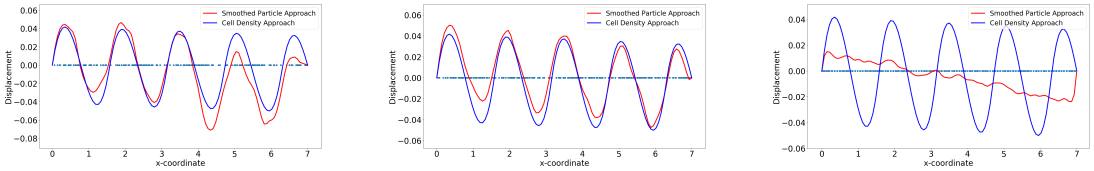

(d) $d(h) = 2h, h = 0.07, d = 0.14$ (e) $d(h) = h, h = 0.07, d = 0.07$ (f) $d(h) = h/4, h = 0.07, d = 0.0175$

Figure 5: The cell density function is sine function and using the algorithm in Figure 2, different simulations are carried out with various mesh size and the total number of cells. Blue curves represent the solutions to (BVP^2_{SP}), and ref curves are the solutions to (BVP^2_{den}) with $n_c(x) = 40|\sin(2x)|$. In Subfigure (a)–(c), we set $d = 0.35$ and cell positions are fixed. From Subfigure (d) to Subfigure (f), we use the same finite-element method settings (where h is efficiently small with $h = 0.07$), and we take different values of d.

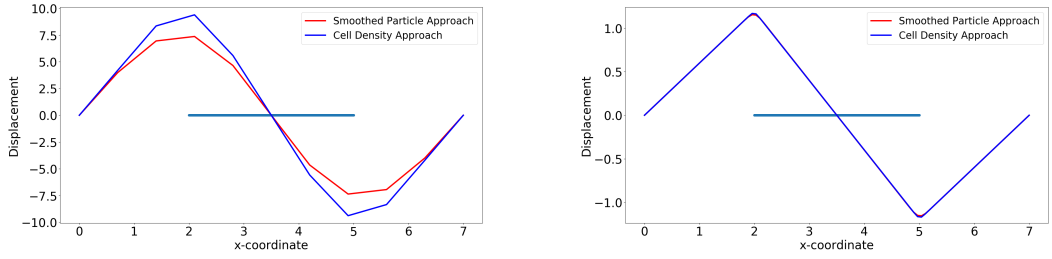

(a) $h = 0.7$ (b) $h = 0.07$

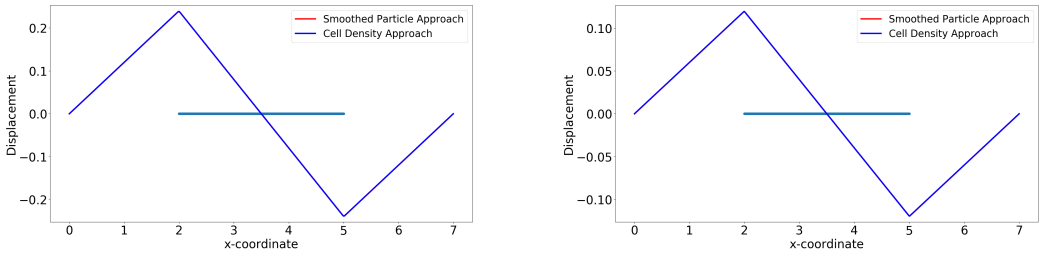

(c) $h = 0.014$ (d) $h = 0.007$

Figure 6: The finite-element method solutions to (BVP^2_{SP}) and (BVP^2_{den}) are shown where cells are uniformly located. With the fixed positions of cells, the solutions are convergent as $h \to 0^+$. Blue points are the centre positions of biological cells. Red curves represent the solutions to (BVP^2_{SP}) and blue curves represent the solutions to (BVP^2_{den}).

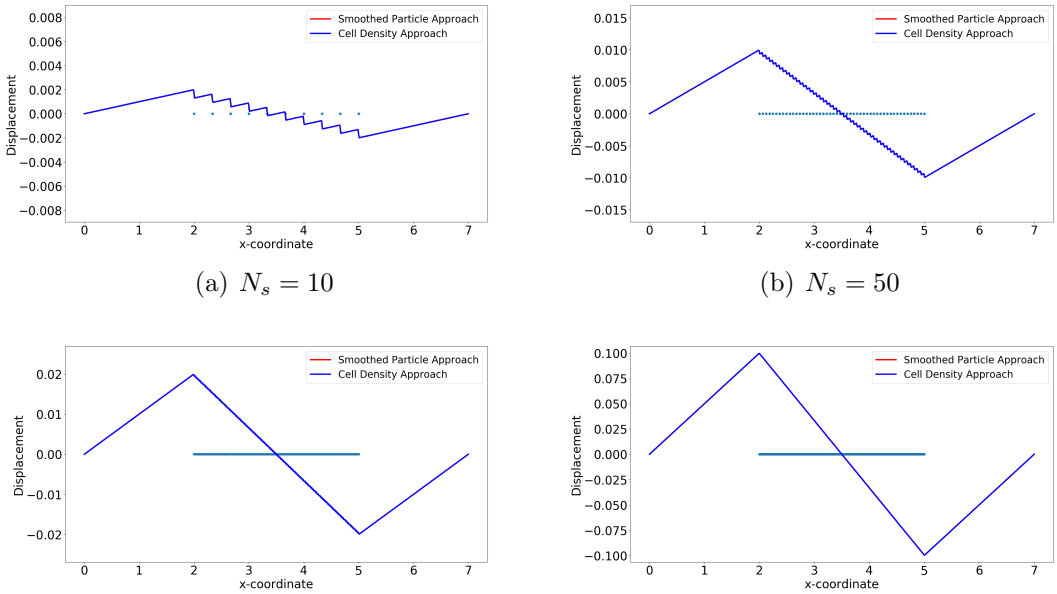

(a) $N_s = 10$ (b) $N_s = 50$

(c) $N_s = 100$ (d) $N_s = 500$

Figure 7: The finite-element method solutions to (BVP^2_{SP}) and (BVP^2_{den}) are shown with uniform distribution. Compared to the analytical result, the consistency between two approaches are unrelated to the number of cells, and the solutions are convergent as $h \to 0^+$. Here, we use $h = 0.007$. Blue points are the centre positions of biological cells. Red curves represent the solutions to (BVP^2_{SP}) and blue curves represent the solutions to (BVP^2_{den}).

Table 2: Numerical results of two approaches in one dimension with biological cells located uniformly. Here, we define mesh size $h = 0.07$ and $N_s = 50$, which means $\Delta s = 0.06$. The results are solved by finite-element method with algorithm in Figure 3.

	SP Approach	**Cell Density Approach**
$\|u\|_{L^2((0,L))}$	0.1858655201	0.1858660118
$\|u\|_{H^1((0,L))}$	0.2780804415	0.2914497482
Convergence rate of $L^2 - norm$	0.9940317098	0.9985295706
Convergence rate of $H^1 - norm$	1.002001685	1.004380036
Reduction ratio of the subdomain (a, b) (%)	7.96908	7.98821
Time cost (s)	0.10391	0.0030458

4 Conclusions

We discussed the link between an agent-based model and a continuum-based model in a one-dimensional setting. For this one-dimensional setting, the exact solution to the problem is known for a specific distributions of the locations of biological cells that pull their immediate environment. Since the Dirac delta functions and its smoothed Gaussian regularization are, de facto, probability density functions, Chebychev's Inequality and the Squeeze Theorem are used to establish convergence between the continuum-based and

agent-based approaches. Furthermore, for Lagrangian linear basis functions, we demonstrate the consistence between both approaches in the finite element space as the element size tends to zero for generic spatial arrangements of the cells. Further efforts in this research will be directed to generalize the mathematical results to higher dimensionality.

Acknowledgment

The authors appreciate China Scholarship Council (CSC) for the financial support for this project.

References

[1] Benjamin Donald Cumming, DLS McElwain, and Zee Upton. A mathematical model of wound healing and subsequent scarring. Journal of The Royal Society Interface, 7(42):19–34, 2009.

[2] Stuart Enoch and David John Leaper. Basic science of wound healing. Surgery (Oxford), 26(2):31–37, 2008.

[3] Eric Haertel, Sabine Werner, and Matthias Schäfer. Transcriptional regulation of wound inflammation. In Seminars in Immunology, volume 26, pages 321–328. Elsevier, 2014.

[4] P. Martin. Wound healing–aiming for perfect skin regeneration. Science, 276(5309): 75–81, April 1997. doi: 10.1126/science.276.5309.75. URL `https://doi.org/10.1126/science.276.5309.75`.

[5] Qiyao Peng and Fred Vermolen. Agent-based modelling and parameter sensitivity analysis with a finite-element method for skin contraction. Biomechanics and Modeling in Mechanobiology, 19(6):2525–2551, July 2020. doi: 10.1007/s10237-020-01354-z. URL `https://doi.org/10.1007/s10237-020-01354-z`.

[6] WM Boon, DC Koppenol, and FJ Vermolen. A multi-agent cell-based model for wound contraction. Journal of biomechanics, 49(8):1388–1401, 2016.

[7] DC Koppenol. Biomedical implications from mathematical models for the simulation of dermal wound healing. 2017.

[8] Qiyao Peng and Fred Vermolen. Numerical methods to solve elasticity problems with point sources. Reports of the Delft Institute of Applied Mathematics, Delft University, the Netherlands, 1389-6520(19-02), 2019.

[9] Qiyao Peng and Fred Vermolen. Point forces and their alternatives in cell-based models for skin contraction. Reports of the Delft Institute of Applied Mathematics, Delft University, the Netherlands, 1389-6520(19-03), 2019.

[10] Dietrich Braess. Finite Elements: Theory, Fast Solvers, and Applications in Solid Mechanics. Cambridge University Press, 2007.

[11] EW Weisstein. Erf. from mathworld—a wolfram web resource. URL: http://mathworld.wolfram.com/Erf.html, 2010.

[12] Richard Haberman. Elementary Applied Partial Differential Equations, volume 987. Prentice Hall Englewood Cliffs, NJ, 1983.

[13] Q. Peng and F. J. Vermolen. Upscaling between an agent-based model (smoothed particle approach) and a continuum-based model for skin contractions, 2021.